Meteoritics & Planetary Science 40, Nr 9/10, 1299–1310 (2005)
Abstract available online at http://meteoritics.org

Experimental shock synthesis of diamonds in a graphite gneiss

Thomas KENKMANN[1*], Ulrich HORNEMANN[2], and Dieter STÖFFLER[1]

[1]Institut für Mineralogie, Museum für Naturkunde, Humboldt-Universität Berlin, Invalidenstrasse 43, D-10115 Berlin, Germany
[2]Fraunhofer Institut für Kurzzeitdynamik, Ernst-Mach Institut, Am Klingelberg 1, D-79588 Efringen-Kirchen, Germany
[*]Corresponding author. E-mail: thomas.kenkmann@rz.hu-berlin.de

(Received 11 June 2003; revision accepted 18 October 2004)

Abstract–The occurrence of diamonds in terrestrial impact craters and meteorites is related to dynamic shock loading during hypervelocity impacts. To understand the mechanism of impact diamond formation in natural rocks, shock-recovery experiments with graphite gneiss were carried out at shock pressures between 35 and 79 GPa. This is the first report on the successful shock synthesis of microdiamonds in a natural rock. Micrometer-size diamonds and a wide range of intermediate, presently unclassified, amorphous, and disordered carbon phases were observed within vesiculated biotite melts in the vicinity of relic graphite grains using microRaman spectrometry. We explain these findings by jetting mechanisms of carbon and graphite clusters, originating at the edges of graphite grains, into the very hot and volatile rich biotitic melt veins during shock loading. This environment enabled the thermally activated crystallization of diamonds during shock compression in a period of less than 0.5 μsec. Regraphitization of diamonds during pressure release was widespread and caused the formation of the amorphous to disordered carbon phases recorded frequently with microRaman spectroscopy. The surviving diamonds must have cooled down to 2000 K during the compression phase at local thermal sinks and cooler interfaces to avoid regraphitization.

INTRODUCTION

Diamonds form in a variety of natural environments for which particular physical conditions can be inferred: high static pressures and high temperatures apply to kimberlitic and metamorphic diamonds (Harris and Gurney 1979; Sobolev and Shatsky 1990) and contrast with dynamic shock pressure pulses for diamonds formed in impact craters (Masaitis et al. 1995; Koeberl et al. 1997) and meteorites (Foot 1891; Miyamoto 1998). Diamond formation by chemical vapor deposition at low pressures and high temperatures is also possible in stellar atmospheres where the nanodiamonds of chondrites (Lewis et al. 1987) were generated. Laboratory synthesis of diamond was accomplished by simulating each of the above physical settings (Bundy et al. 1955; DeCarli, and Jamieson 1961; Angus and Hayman 1988).

The early findings of diamond in meteorites stimulated experimental shock investigations. For the formation of diamonds by experimental shock, mixtures of porous carbon, copper (for purposes of rapid quenching), and explosives have been used (DeCarli 1995). The successful synthesis of diamond and lonsdaleite (a hexagonal diamond polymorph) by shock wave experiments was first reported by DeCarli and Jamieson (1961). This method is now widely commercialized. Subsequently, natural diamonds were also discovered in terrestrial impact structures, e.g., at the Popigai crater (Masaitis et al. 1995; Koeberl et al. 1997; Masaitis 1998), the Ries crater (Hough et al. 1995; El Goresy et al. 2001; Schmitt et al. 2005), and within the globally distributed Chicxulub ejecta layer at the Cretaceous-Tertiary boundary (Gilmour et al. 1992). Diamonds of the Popigai impact structure were found in strongly shocked gneiss fragments contained in suevites and impact melt rock. They typically occur as polycrystalline aggregates, which preserve the crystal habit of the precursor graphite grains and thus represent paramorphs after graphite. This indicates that they were formed by a shock-induced, solid-state, martensitic transformation of graphite to diamond (Koeberl et al. 1997; Masaitis 1998). Masaitis (1998) distinguished between authigenic diamonds (located at their place of origin within gneiss fragments) and allogenic diamonds that are dispersed in impact melts. In situ findings of diamonds in shocked graphite-bearing gneiss fragments from the suevite of the Ries crater (El Goresy et al. 2001) indicate that diamond aggregates formed within weakly deformed graphite grains at those sites that are in contact with relatively denser, neighboring minerals such as garnet and sillimanite. This

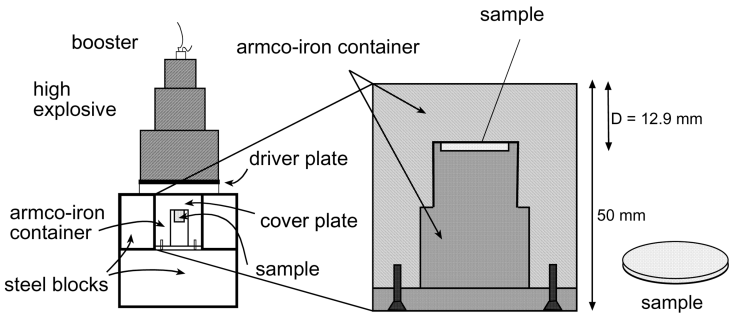

Fig. 1. Experimental setup of the shock recovery experiments using the multiple reverberation technique.

(a) (b)

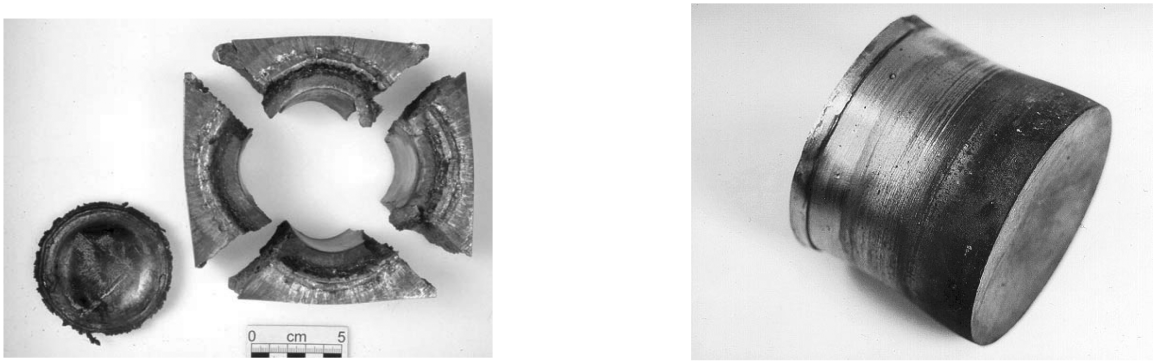

Fig. 2. a) Driver plate and steel blocks after deformation; b) Armco-iron container after deformation at 45 GPa.

Table 1. Details of the shock recovery experiments.

Experiment	Cover plate thickness (mm)	Flyer plate thickness (mm)	Explosive	Pressure (GPa)	Pre-impact temp. (°C)
1[a]	8.2	4	Comp. B	35	20
2[a]	6.6	3	Comp. B	45	20
3[b]	6.5	3	Comp. B/octogen	69	20
4[b]	8.2	2	Comp. B/octogen	79	20

[a]64 mm explosive device; container 100 × 100 × 50 mm.
[b]80 mm explosive device; container 120 × 120 × 50 mm.

occurrence was attributed to impedance contrasts at phase boundaries (El Goresy et al. 2001). Recently, El Goresy et al. (2002; 2003) reported a new transparent, very hard polymorph of carbon from the Ries and Popigai craters.

Based on shock experiments, DeCarli (1995) reported that above 15 GPa and 1300–2000 K, cubic and hexagonal diamonds can be made from well-ordered graphite by a quasi-diffusionless (martensitic) transformation mechanism. However, at temperatures above 3000 K, cubic diamond can eventually be formed by thermally activated nucleation and growth mechanisms, provided that the newly formed phases are quenched to low temperatures before the pressure decays into the graphite stability field.

To unravel the nature of the graphite-diamond shock transformation, we performed shock recovery experiments (Figs. 1 and 2, Table 1). Attempting to reproduce a realistic, natural scenario, we used a natural rock (Fig. 3) instead of an artificial aggregate of graphite powder, copper, and high explosive. The pressure range of the experiments was 35–79 GPa (Fig. 4, Table 1) which matches the natural conditions under which suevitic rocks form, but the pressure pulse duration in the experiments (0.3–0.8 μsec) is lower by up to six orders of magnitude compared to large-scale impact events. Nevertheless, it was possible to produce microdiamonds and other as yet unclassified carbon phases in a natural rock by shock-loading experiments for the first time.

STARTING MATERIAL, EXPERIMENTAL SETUP, AND ANALYTICAL TECHNIQUES

For our shock experiments, we used a recovery technique that maintained the textural context of the rock. After

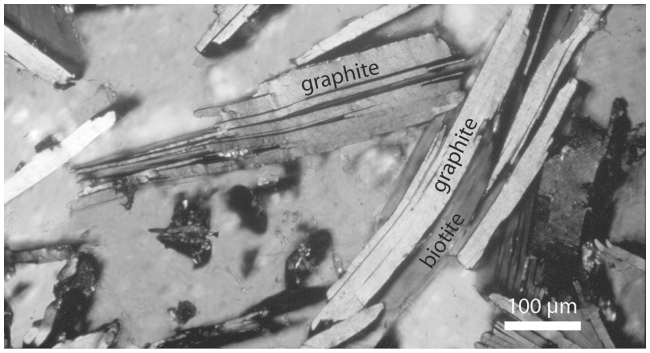

Fig. 3. Graphite gneiss, unshocked (reflected light, crossed nicols). Note the intergrowth of biotite and graphite along their basal planes.

preparation of the thin sections, this technique allowed an in situ study of diamond formation. The starting material was a graphite gneiss from Kropfmühl in southern Germany (Fig. 3). This gneiss consists of ~47 vol% graphite, ~35 vol% plagioclase, ~10 vol% quartz, and ~5 vol% biotite, and ~3 vol% pyrite. The bulk chemical composition is given in Table 2. The gneiss displays an irregular foliation at the scale of centimeters. Graphite and biotite are mostly intergrown parallel to their basal planes (Fig. 3). The average grain size of graphite and its ellipticity (ratio of long to short grain axis) in foliation-parallel sections is 116 µm and 3.0, respectively. The irregular foliation affords various orientations of the graphite grains with respect to the incoming shock wave in any given sample. The mineral constituents and fabric of the rock are similar to gneisses of the Popigai and Ries craters that contain natural shock-induced diamonds (Masaitis et al. 1995; Koeberl et al. 1997; Masaitis 1998; El Goresy et al. 2001). However, the quantity of graphite in our samples clearly surpasses the gneisses of the Ries and Popigai craters.

For the shock recovery experiments, we used cylindrical discs 15 mm in diameter and 0.5 mm in thickness (Figs. 1 and 2). A multiple reverberation technique was used to achieve pressures of 35, 45, 69, and 79 GPa in the samples, respectively (Fig. 4a, Table 1). The detonation of a high explosive plane wave generator accelerated a flyer plate into the flat surface of an ARMCO-iron container in which the sample disc was embedded. Different shock pressure levels were achieved in this pressure calibrated assembly (Müller and Hornemann 1969) by varying the type of explosive (Composition B or Composition B/octogen) and by changing the thickness of the flyer plate (2–4 mm) and cover plate (6.5 or 8.2 mm), respectively (Table 1) (for pressure calibration, see also Stöffler and Langenhorst 1994). A stepwise increase in shock pressure within the sample is accomplished by multiple reverberations of the shock wave at the bottom and top contact with the iron container, as illustrated in Fig. 4a. The duration of the peak pressure decreases with increasing shock because of the use of a thinner flyper plate (Table 1). A basic interpretation of the Hugoniot curves, such as the one in Fig. 4a, is given in Stöffler and Langenhorst (1994). The

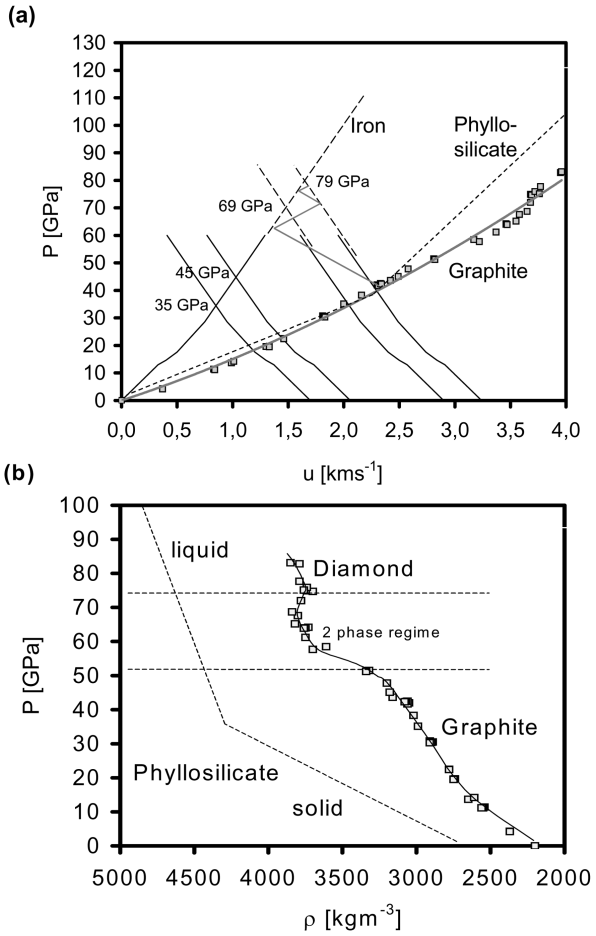

Fig. 4. a) Hugoniot curves of phyllosilicate (shale) (Trunin 2001), graphite (Stöffler 1982), and Armco-iron (sample container) for calculation of the final equilibrium pressure achieved by the reverberation technique. *P* is shock pressure and *u* is particle velocity. b) Hugoniot data for graphite-diamond transition as displayed in Stöffler (1982) and for phyllosilicate (shale) (Trunin 2001). *P* is shock pressure and ρ is density of the shocked mineral.

Table 2. Bulk composition of the starting material.

Graphite gneiss, Kropfmühl, Germany	
SiO_2	48.3
TiO_2	0.27
Al_2O_3	10.6
Fe_2O_3	5.08
MnO	0.04
MgO	0.72
CaO	2.69
Na_2O	3.29
K_2O	0.42
P_2O_5	0.16
LOI	27.7
Sum	99.27 wt%

Hugoniot curve for graphite indicates that a phase transition to diamond mainly occurs at a shock pressure interval of 45–70 GPa (Fig. 4b).

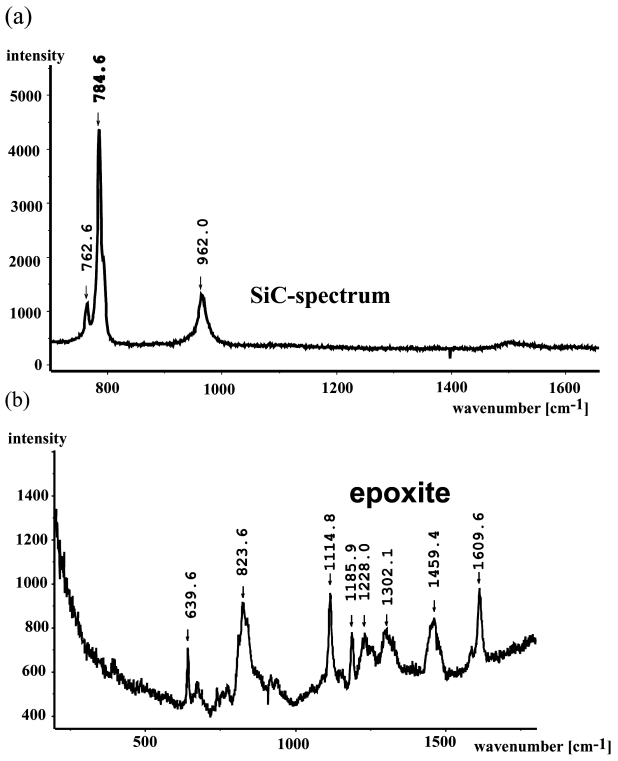

Fig. 5. Raman spectra of a) grinding and polishing paste and b) epoxy used for the preparation of thin sections.

We used a lathe to remove the deformed iron container and to recover the sample discs. After impregnation with epoxy under vacuum, thin sections were carefully prepared. The thin section of the 45 GPa sample was ground and polished with SiC, whereas the other samples were prepared conventionally. The samples were analyzed using optical microscopy and microRaman spectrometry. Scanning electron microscopy (SEM) and electron microprobe mapping of the 45 GPa sample with a wavelength-dispersive spectrometer were performed without conductive coating at 15 kV and a low current of 6×10^{-10} A to avoid charging of the sample.

Confocal microRaman spectrometry was carried out with a notch filter-based Dilor LabRam system equipped with an HeNe laser (632.8 nm), a 50× and 100× microscope lens, and a scanning device. The focused laser beam had a spot diameter of ~1 µm; the wavenumber accuracy is about 1 cm^{-1}. The laser beam was focused ~1–2 µm below the section surface to avoid possible artifacts of grinding and polishing. All investigations were carried out after removal of the background and subsequent Gauss-Lorentzian fitting of bands. According to the software package LabSpec, the following algorithm is used for the fitting procedure:

$$y = a \bullet (g \bullet \exp(-(x-p)^2))/(w^2) + (1-g)/1 + 4 \bullet ((x-p)^2)/w^2 \quad (1)$$

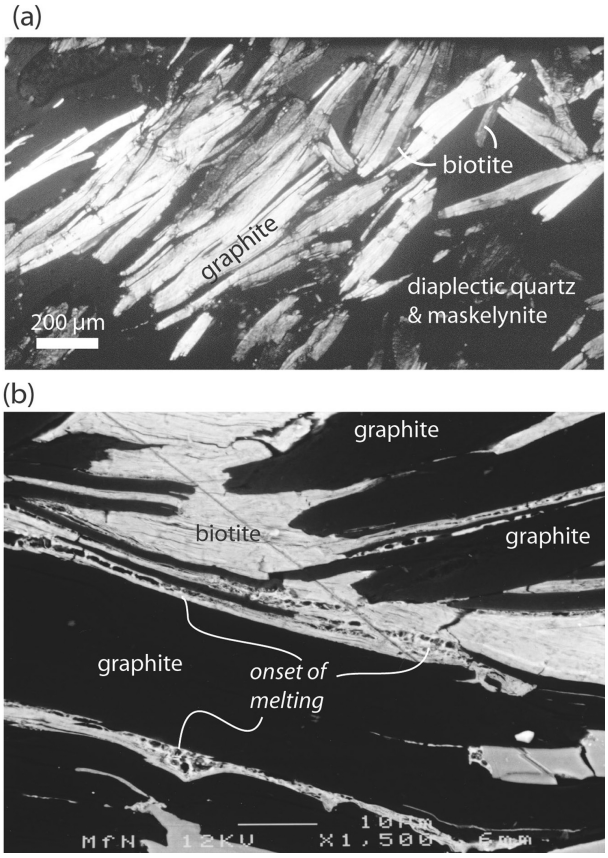

Fig. 6. Graphite gneiss (35 GPa). a) Biotite still displays birefringence. Quartz and plagioclase are transformed to diaplectic glasses (reflected light, crossed polarizers). b) Vesicular melting of biotite occurs at the interfaces with graphite (SEM-BSE; backscattered electrons).

In this algorithm, p is the central value of a band, w is the width at half maximum, and g is the ratio of the Gaussian and Lorentzian fitting procedure, which are calculated separately.

As the thin sections were analyzed, the superposition of graphite and diamond Raman bands by those of epoxy and the grinding material cannot be completely excluded (Fig. 5). Epoxy spectra show many peaks, three of which (1302 cm^{-1}, 1459 cm^{-1}, and 1609 cm^{-1}) may locally influence the amplitude of carbon spectra (Fig. 5b). However, a possible superposition can easily be identified by the presence or absence of other epoxy bands that do not overlap with graphite bands. The spectrum of SiC (Fig. 5a), used as grinding and polishing paste, does not show any Raman bands in the wavenumber region of interest for the graphite-diamond transformation (1300–1600 cm^{-1}).

RESULTS

Optical and SEM analyses show that graphite grains survived in all experiments, but they become heavily kinked, twinned, and otherwise deformed with increasing pressure,

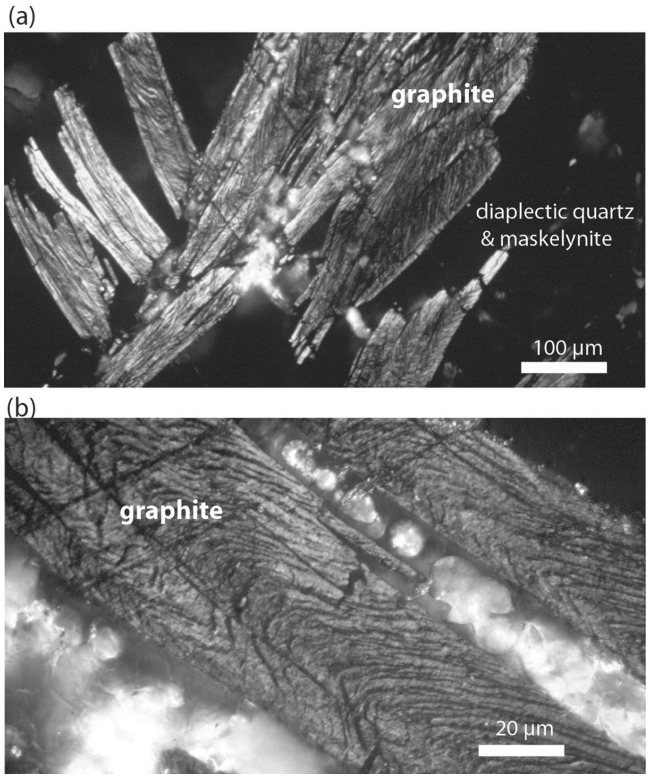

Fig. 7. Graphite gneiss (69 GPa, reflected light, crossed polarizers). Relic graphite grains display many kink bands. The bright spots indicate vesicular melts (arrows) that surround the graphite grains. This melt contains various carbon phases, including diamond.

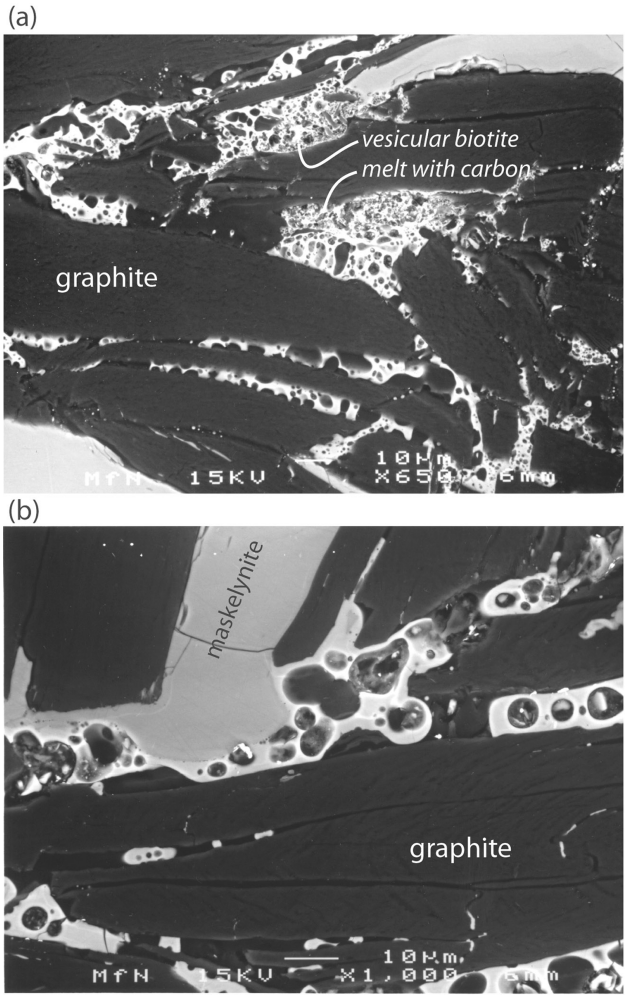

Fig. 8. Graphite gneiss (69 GPa, SEM-BSE). Biotitic melt surrounds heavily deformed graphite grains and intrudes along the basal planes of graphite.

pending on their orientation with respect to the incoming shock wave (Figs. 6–8). Plagioclase and quartz are transformed to diaplectic glass in the experiments, in general agreement with previous studies (Stöffler and Langenhorst 1994). However, in the 35 GPa experiment, small domains of quartz still show a weak birefringence (Fig. 6a) and display abundant planar deformation features. The incomplete transformation to diaplectic quartz glass may indicate local disturbances of the shock wave induced by impedance contrasts of adjacent grains. The given shock magnitudes, therefore, merely reflect a mean value achieved in an experiment. Deviations of up to a few gigapascal near grain boundaries are possible, as other studies have shown (Kenkmann et al. 2000; Heider and Kenkmann 2003). Also, deviation from planar shock wave geometry can occur near the edges of the cylindrical samples, where slightly higher shock pressures can be inferred from the observed shock metamorphic effects. Biotite persists in the crystalline state after the 35 GPa experiment, but to a lesser degree after the 45 GPa experiment. Melting of biotite at 35 GPa is restricted to graphite-biotite grain boundaries (Fig. 6b). This observation is in agreement with shock experiments on micas. Lambert (1984) reported a beginning vesiculation of biotite at 32 GPa. This is also in accordance with Hugoniot data for phyllosilicates (shale) (Trunin 2001). Figure 4a shows a remarkable change in slope of the Hugoniot curve at a pressure of ~37 GPa, which corresponds with the transition of solid-state deformation to a high pressure liquid (melt). The preferred melting of biotite at graphite-biotite interfaces in the 35 GPa experiment is caused by impedance contrasts between the neighboring mineral phases and shear heating. Perturbation of the planar shock wave (reflection, refraction, and interference) at phase boundaries produces localized excursions in temperature, strain, and pressure (Hertzsch et al. 2005; Heider and Kenkmann 2003). At 69 and 79 GPa, biotite is completely melted (Figs. 7 and 8). Melting is indicated by schlieren and the presence of vesicles. The latter indicates vaporization and release of water during pressure decay (Fig. 8). As biotite is initially intergrown with graphite, this melt occurs in contact to the relic graphite grains. It often intrudes into cracks perpendicular to the basal planes of graphite. Melt veins also form bridges between neighboring

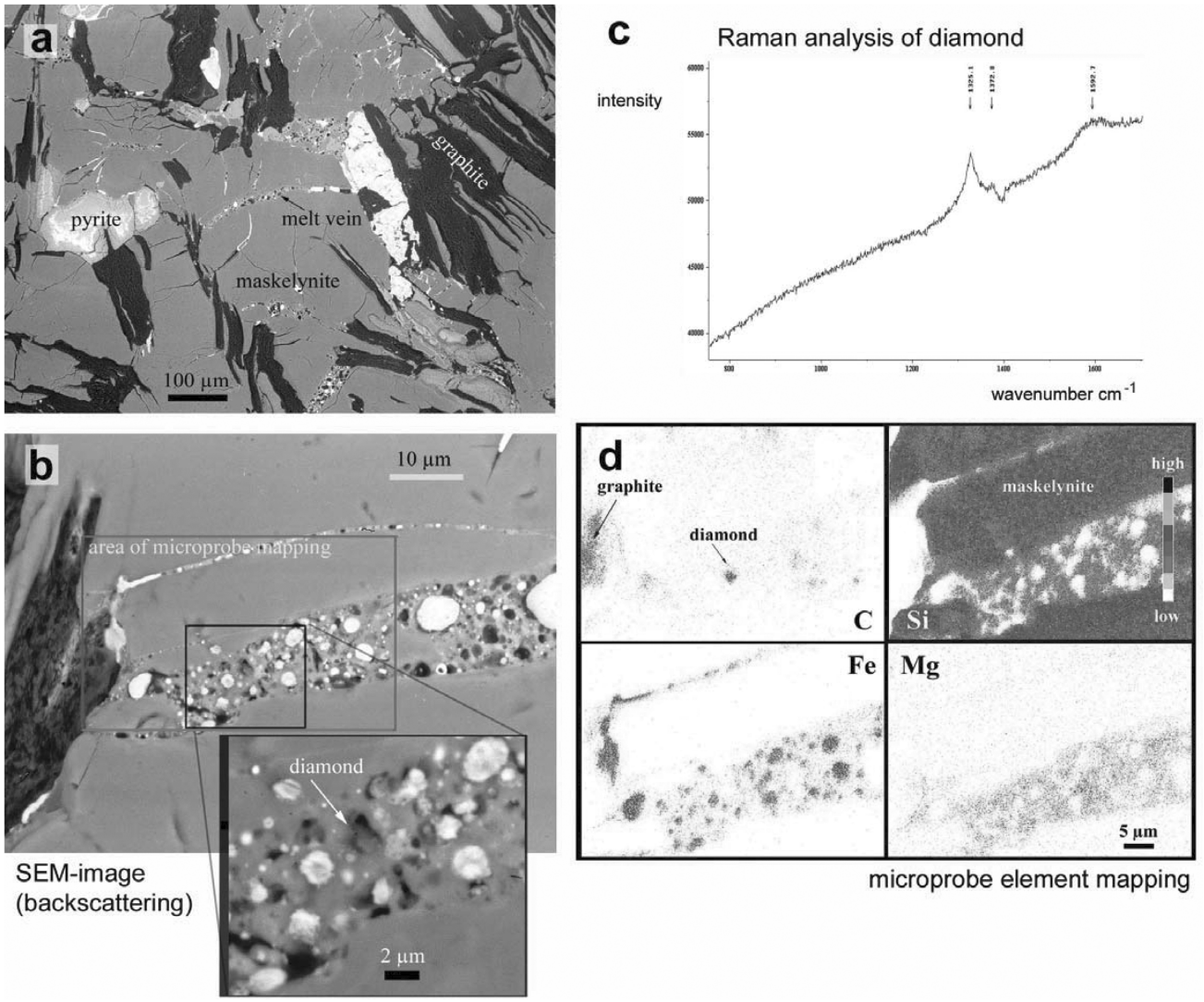

Fig. 9. Graphite gneiss after shock loading at 45 GPa. a) The SEM-BSE image shows the typical fabric of the graphite gneiss. Graphite grains and a few large pyrite grains are surrounded by maskelynite and diaplectic quartz. Note the distribution of the vesicular melt veins forming bridges between graphite grains and pyrite. b) The enlarged melt vein of (a) contains irregularly shaped inclusions and vesicles. A 1.5 µm diamond grain (most probably a nano-diamond aggregate) was found within the melt vein. c) This particular diamond grain is indicated by a sharp Raman band at 1325 cm^{-1} with a FWHM of 33 cm^{-1}. d) Microprobe element mapping of the melt vein indicates a biotite-like composition with additional C and Fe incorporated into the melt. The locations of carbon concentration correspond to the diamond grain and other disordered carbon phases.

graphite aggregates (Fig. 9). The composition of the melt veins enlarged in Fig. 9b deviates from a biotite-normative character insofar as C, Ca, and Fe are enriched to a variable degrees (Fig. 9d).

It is in this melt that different carbon phases, including diamond, were discovered by Raman spectroscopy (Fig. 9c). Near the edges of the sample, Fe from the iron container can contaminate the melt (Figs. 9b and 9d), but diamonds were observed irrespective of this additional effect. Carbon aggregates are present within the melt veins (Fig. 9). The amount of melt and the quantity of carbon aggregates become more voluminous with increasing pressure (cf. Figs. 6b and 8a). The carbon aggregates primarily consist of disordered graphite, amorphous carbon, and, to a small degree, dispersed diamonds. Diamonds are typically very small (~1 µm). Graphite paramorphs of diamond have not been observed.

Identification of the different carbon phases was achieved by Raman analysis. The first-order Raman band (F_{2g}) of diamond occurs at wavenumber 1332 cm^{-1} and represents the main C-C bond vibration in diamond. A shift of this Raman peak to lower wavenumbers is a well-known effect occurring at very small crystallite sizes (Zhao et al. 1998). It can also vary as a function of lattice stress, presence of lonsdaleite, or of temperature, which, in turn, depends on the incident laser power (Miyamoto 1998). In our experiments, the diamond Raman peak is located in the

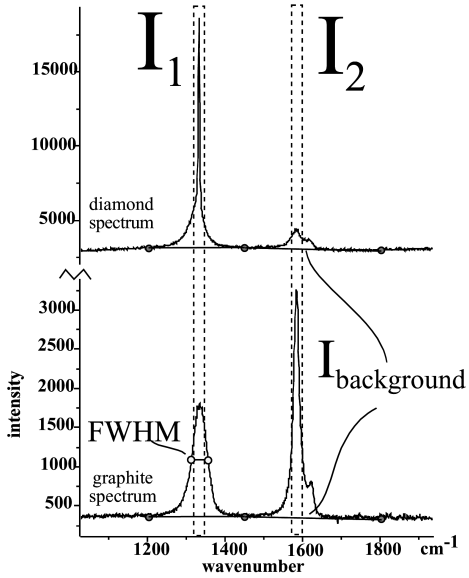

Fig. 10. Systematic analysis of diamond and graphite spectra is based on the I_1/I_2 ratio, FWHM, $I_1/I_{background}$ and the wavenumber of the I_1 and I_2 bands.

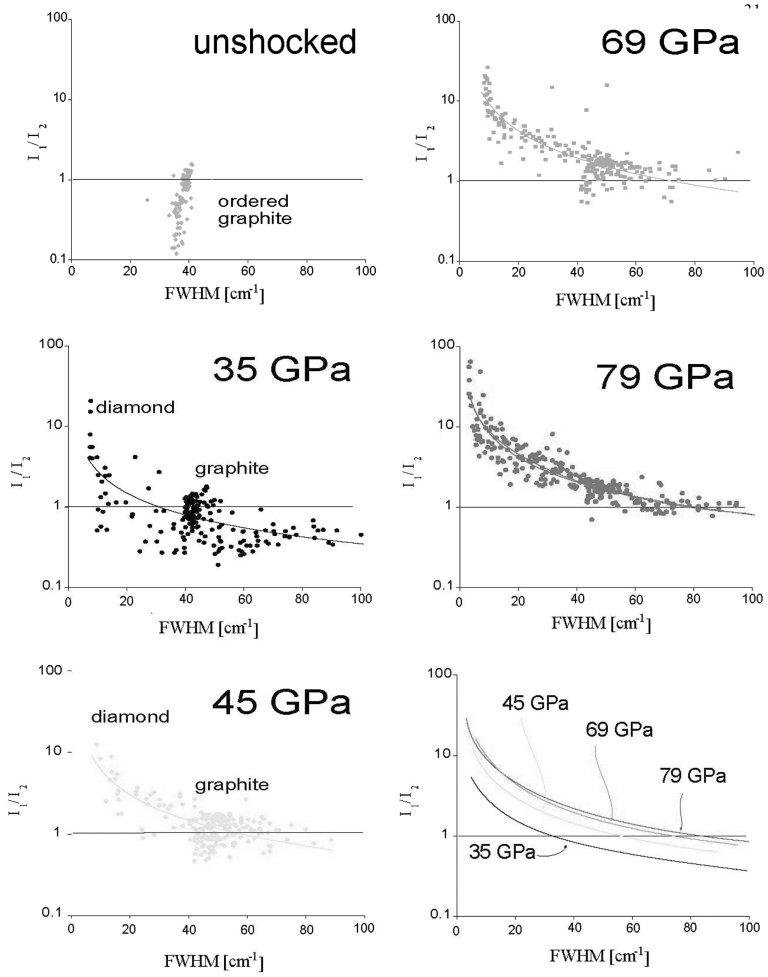

Fig. 11. Analyses of I_1/I_2 versus FWHM for all Raman spectra of graphite, diamond, and intermediate carbon phases. The regression lines show a systematic shift to higher I_1/I_2 ratio for a given FWHM with increasing shock (see text).

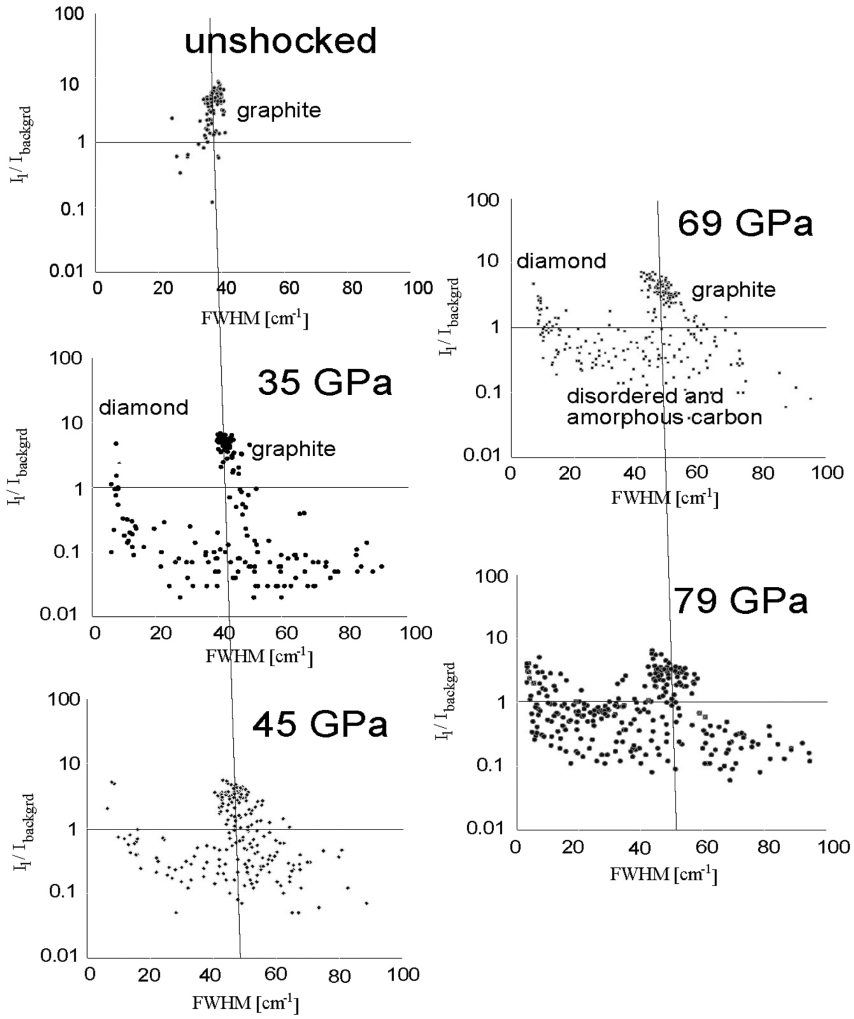

Fig. 12. Analyses of $I_1/I_{background}$ versus FWHM for all Raman spectra of graphite, diamond, and intermediate carbon phases. The bands of persisting graphite become progressively broader with increasing shock. Also, intermediate carbon phases become more abundant with increasing shock (see text for discussion).

interval 1317–1332 cm^{-1}. The width of the diamond peak, expressed as the full width at half maximum (FWHM), mainly reflects the degree of crystal structure order (Miyamoto 1998). FWHM varies with the mode of diamond synthesis, with 2–3 cm^{-1} being typical for static high pressure diamonds, 3–25 cm^{-1} indicating CVD diamonds, and 10–120 cm^{-1} being characteristic for shock-induced diamonds (Miyamoto 1998). We measured FWHM down to 10 cm^{-1} in the 45 GPa experiment. Graphite can be identified by the dominance of the 1581 cm^{-1} band. Depending on the degree of disordering and orientation of the graphite grain, a second band around 1350 cm^{-1} and a shoulder at 1620 cm^{-1} of lower intensity is present. The relative intensities of the 1350 cm^{-1} and 1581 cm^{-1} peaks and their FWHM reflect the degree of ordering (El Goresy et al. 2001), but this ratio is also affected by the orientation of the incident beam with respect to the graphite basal plane. Our Raman analysis showed a general shift of the 1350 cm^{-1} band to lower wavenumbers, even in the unshocked sample. We also found a continuous transition between the 1332 cm^{-1} diamond band and the 1350 cm^{-1} graphite band. In the following, the band at 1317–1350 cm^{-1} band is denoted as I_1, and the 1581 cm^{-1} band as I_2 (Fig. 10). To characterize the phase transformation from graphite to diamond, we recorded the I_1/I_2 ratio after removal of the background, the ratio of I_1 intensity to background intensity, FWHM, and the wavenumber of the bands (Fig. 10).

With increasing pressure, the Raman spectra of relic graphite display an increase of the I_1/I_2 ratio (Fig. 11) and a decrease in the intensity of both bands with respect to the background signal (Fig. 12). I_1 shows a shift to lower wavenumbers and a weak broadening from ~38.5 cm^{-1} (unshocked) to 47.0 cm^{-1} (79 GPa) FWHM (Fig. 12). The increasing magnitude of the background documents an increasingly disordered state of graphite with increasing pressure. Our analysis particularly focused on the dispersed carbon phases within the melt veins. Spectra of these

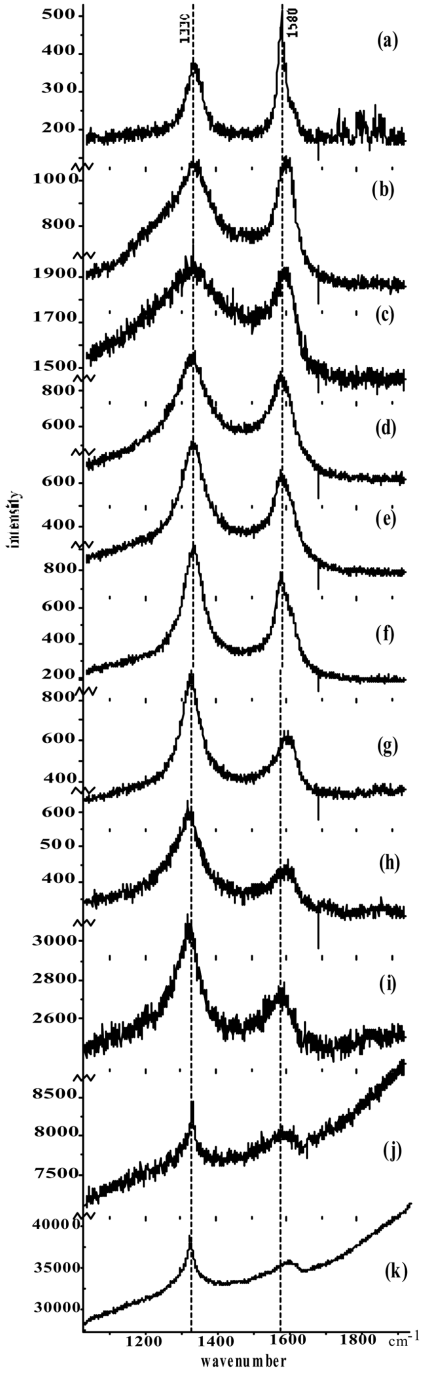

Fig. 13. Raman spectra of relic graphite (a), diamond (j, k), and intermediate disordered carbon phases at 45 GPa. All spectra were measured in a single melt vein. A gradational transition from a graphite spectrum (a) to a diamond spectrum (j, k) is seen. With progressive transformation, the first band becomes very broad (FWHM ~150 cm^{-1}) and increases in relative intensity indicating structural disorder. The large background signal between the major bands is interpreted as progressive amorphization. While the intensity of the first band progessively increases, the full width at half maximum (FWHM) decreases from 150 to 34 cm^{-1}. Eventually, fluorescence starts to develop. This is very typical for diamond and leads to an enhanced count rate (j, k).

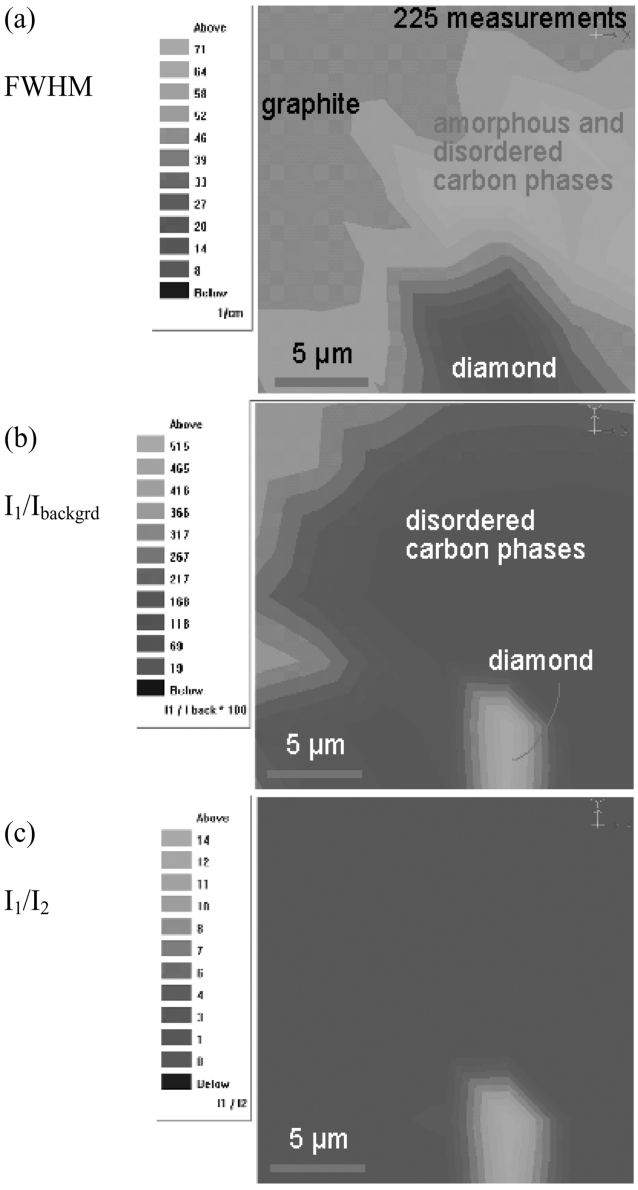

Fig. 14. Results of a 15 × 15 Raman-scanning of an area of ~400 μm^2 The step size is 1.3 µm. a) FWHM of I_1. b) I_1 /$I_{background}$. c) I_1/I^2. Domains of relic graphite (upper left) and diamond (lower right) are separated by a zone of disordered carbon phases with a high background signal and broad I_1 bands.

dispersed carbon phases are highly variable, within one sample and even within a single melt vein. Figure 13 displays the range of carbon spectra found in the sample that experienced a nominal pressure of 45 GPa. The order of the spectra in Fig. 13 reflects a spatial context of measurements found in Raman scans. Taking the width of the Raman bands as a measure of the degree of crystal-structure disorder, a continuous range of spectra exists between graphite (Fig. 13a), disordered to amorphous graphite-like carbon (Figs. 13b–i), and diamond (Figs. 13j–k) of variable order. The peak maximum of the I_1 band is at 1328 cm^{-1}, on

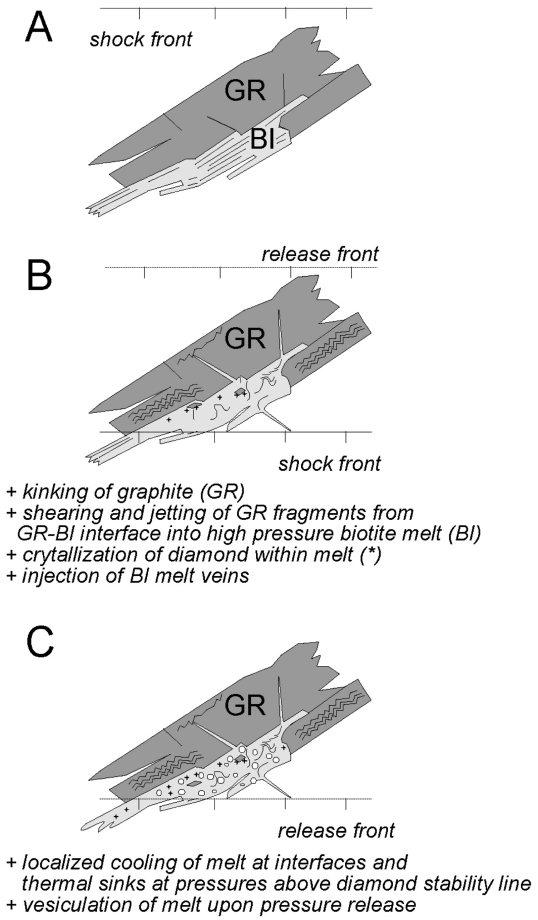

Fig. 15. Schematic sketch displaying the formation of diamonds. See text for discussion.

average, but it can occur between 1317 and 1345 cm^{-1}. The shift from 1332 cm^{-1} toward lower wavenumbers may indicate that diamonds, such as the one in Fig. 9b, are of submicron size and form polycrystalline aggregates, although this is beyond the resolution of the technique used. The spectra of graphite, diamond, and intermediate phases differ with respect to the background. With respect to absolute intensities, graphite has a very low background, intermediate phases an enhanced background, and diamond a very strong background, indicating progressive fluorescence (Figs. 12 and 13). With respect to relative intensities, amorphous graphite-like carbon has the highest background signal with respect to I_1. The spatial context of relic graphite grains, diamond, and disordered to amorphous carbon phases is illustrated in Fig. 14. Diamond, characterized by a small FWHM and a high I_1/I_2 ratio is surrounded by disordered carbon phases, which display a large background signal and very broad bands. There is no apparent spatial connection of the relic graphite grain and the microdiamond (Fig. 12).

Although a remarkable variety of carbon phases co-exist at a single shock level within the melt veins, it is possible to identify systematic trends from low to high shock pressure by considering regression lines (Fig. 11) (Kenkmann et al. 2002). The relationship between FWHM and the I_1/I_2 ratio obeys a power law of the form: $I_1/I_2 = A \bullet FWHM^{-b}$. The pre-exponent factor A ranges between ~22 (35 GPa) and ~120 (69 GPa), while b ranges between 0.9 (35 GPa) and 1.18 (69 GPa) (Fig. 13). This indicates that, at a given FWHM, the I_1/I_2 ratio increases with increasing pressure. In other words, the first band becomes more and more prominent with increasing shock pressure. It is also evident that the average $I_1/I_{background}$ ratio of disordered carbon phases increases with increasing shock pressure from about 0.05 (35 GPa) to 0.4 (79 GPa) (Fig. 12). As the transition between the graphite spectra and diamond spectra is gradational, it is difficult to identify the exact boundary between graphite phases, disordered carbon phases, and diamond phases.

DISCUSSION

Diamond formation in the experiments is restricted to melt veins. Evidence for an in situ martensitic, solid-state transformation of graphite to diamond within persisting graphite grains or at graphite boundaries was not observed. The locations where diamonds are discovered are several micrometers away from possible graphite hosts and indicate an injection process of graphite or carbon clusters into the melt veins with subsequent or simultaneous formation of microdiamonds. This observation contrasts with the findings of El Goresy et al. (2001), who found impact diamonds in immediate contact to graphite grains in naturally shocked rocks. The Raman investigation showed that a broad range of intermediate carbon structures co-exists between relic graphite grains and diamond. A martensitic transformation process cannot explain this gradational change. As diamonds exclusively reside in melt veins, it is this biotitic melt that may potentially catalyze the reaction or provides suitable conditions for formation and/or preservation of diamond during pressure release. We favor a thermally activated formation mechanism of diamond as earlier proposed by DeCarli (1995). DeCarli (1995) suggests that cubic diamond can be formed at temperatures above 3000 K, by thermally activated nucleation and growth mechanisms, provided the newly formed phases are quenched to lower temperature of 2000 K before the pressure-regime decays into the stability field of graphite. DeCarli (1995) calculated a shock temperature of about 3700 K to account for the growth of 10 nm diamond crystals within a microsecond. This growth time is similar to the period of shock compression in our experiments.

A number of high-pressure minerals (stishovite, hollandites, akimotoite, majorite, etc.) have recently been found in melt veins in meteorites (e.g., Chen et al. 1996; Langenhorst and Poirier 2000) that constrain the mechanisms and PTt conditions during high-pressure phase formation

within melts. Langenhorst and Poirier (2000) showed that high-pressure minerals crystallize directly from the melt under high pressure at very high temperatures. They inferred that crystallization and solidification of the melt veins occurs in extremely short times, much shorter than the duration of the shock.

The melt veins of our experiments differ from those described above in two fundamental aspects. First, they are not primarily the result of adiabatic shear heating and shock pressure excursions. Instead, melting is caused by the dynamic properties of biotite. Figure 4 indicates that the transition from solid-state deformation to a high pressure liquid phase occurs at ~37 GPa. Second, the vesicular texture of the melt clearly indicates that the melt remained, at least in part, liquid upon pressure release. Vesiculation of the biotitic melt is interpreted as primarily the result of H_2O vapor unmixing from the mica liquid under pressure release (Lambert 1984). Prior to this release, the volatiles were dissolved in the liquid melt and may have enhanced diffusion processes within the melt.

Proposed Scenario of Diamond Formation

Figure 15 schematically displays the proposed evolution of processes that lead to the formation of diamond and the other yet unclassified carbon phases in three time steps:

1. The intergrowth of graphite and biotite, which is common in the studied samples, is an important prerequisite for the graphite transformation during shock compression. It is also worth noting that some open fractures and fissures occur in the sample.
2. Shock loading leads to various deformation features in graphite, including intense kink band formation, but graphite grains persist in all experiments. Local pressure and temperature spikes may transiently evolve at graphite-biotite interfaces and develop from the implosive closure of microfractures and fissures (Heider and Kenkmann 2003). Both processes can cause hot spot formation and induce shearing, fragmentation, and jetting of deformed or amorphous graphite fragments of submicron-mm size from the graphite-biotite interface into the adjacent minerals. High pressure melting of biotite is restricted to phase boundaries at 35 GPa, but is complete at 69 GPa. The melt has a low viscosity, as indicated by frequent injections. The high pressure melt with distributed carbon clusters is sufficiently hot (3000–4000 K) to initiate rapid nucleation and growth of nanometer-size diamonds. The dissolved volatiles may enhance the diffusivity of carbon within the melt, which has a positive effect on the reaction kinetics.
3. The release wave ceases the period of shock compression. The majority of diamonds formed during shock compression are probably affected by regraphitization and/or amorphization. Amorphization is a well-known decompression effect and explains the broad bands and high background signals of many Raman spectra of carbon phases (Figs. 11–14). At local thermal inhomogeneities in the melt (thermal sinks, cool interfaces), surviving diamonds are already probably cooled down to 2000 K during the compression phase. This temperature is sufficient to avoid regraphitization (DeCarli 1995). At rather low pressures, unmixing of volatiles from the melt occurs and leads to vesicular texture of the melt.

CONCLUSIONS

This is the first successful experimental shock synthesis of diamond using a natural rock sample. The study shows that highly shocked graphite gneisses or graphite-bearing gneisses are potential carriers of diamonds in impact craters, as observed by Masaitis et al. (1995), Koeberl et al. (1997), Masaitis (1998), and El Goresy et al. (2001). While a martensitic transformation process of graphite to diamond can be inferred from natural rocks for moderate shock pressures of up to 40 GPa (Koeberl et al. 1997; El Goresy et al. 2001), this study demonstrates that additional mechanisms may operate at higher pressures if volatile-rich melts are present in the vicinity of graphite. Diamonds found in melt clasts and metamorphic rock fragments of shock stage III (Stöffler 1971) in fallout suevite of the Ries and Popigai craters are probably formed in this manner. This mechanism requires the presence of very hot melts in contact with the persisting graphite grains. The change in the transformation mechanism from a solid-state-martensitic process to a thermally activated nucleation-and-growth scenario correlates with the onset of melting of biotite.

Acknowledgments–We acknowledge the support and expertise of the Ernst-Mach-Institute, Efringen-Kirchen, Germany, in performing the shock recovery experiments. We are indebted to H. Schneider, H. R. Knöfler (MfN), Mr. Güdemann (EMI), and the preparation lab of the University of Münster, Germany for their technical support. We wish to thank L. Hecht (MfN) for analytical help with the microprobe and B. A. Ivanov (Institute of Geospheres, Moscow) and R.T. Schmitt (MfN) for fruitful discussions. We are grateful to W. U. Reimold and C. Koeberl, who reviewed an earlier version of this paper, and to reviewer F. Hörz, who provided very fruitful input.

Editorial Handling—Dr. Richard Grieve

REFERENCES

Angus J. C. and Hayman C. C. 1988. Diamonds and diamond-like carbon coatings. *Science* 241:913.

Bundy F. P., Hall H. T., and Strong H. M. 1955. Man-made diamonds. *Nature* 176:51–55.

Chen M., Sharp T. G., El Goresy A., Wopenka B., and Xie X. 1996. The majorite-pyrope and magnesiowüstite assemblage: Constraints

on the history of shock veins in chondrites. *Science* 271:1570–1573.

DeCarli P. S. 1995. Shock wave synthesis of diamond and other phases. *Material Research Society Proceedings* 383:21–31.

DeCarli P. S. and Jamieson J. C. 1961. Formation of diamond by explosive shock. *Science* 133:1821–1822.

El Goresy A., Gillet P., Chen M., Künstler F., Graup G., and Stähle V. 2001. In situ discovery of shock-induced graphite-diamond phase transition in gneisses from the Ries Crater, Germany. *American Mineralogist* 86:611–621.

El Goresy A., Gillet P., Mostefaoui S., Chen M., Graup G., and Masaitis V. L. 2002. A transparent, very hard, dense, and unusually disordered form of carbon in heavily shocked gneises from Popigai, Russia: Petrographic settings and comparison with a similar phase in shocked gneisses from the Ries (abstract #1031). 33rd Lunar and Planetary Science Conference. CD-ROM.

El Goresy A., Dubrovinsky L. S., Gillet P., Mostefaoui S., Graup G., Drakopoulos M., Simionovici A. S., Swamy V., and Masaitis V. L. 2003.A novel cubic, transparent and super-hard polymorph of carbon from the Ries and Popigai craters: Implications to understanding dynamic-induced natural high-pressure phase transitions in the carbon system (abstract #1016). 34th Lunar and Planetary Science Conference. CD-ROM.

Foot A. E. 1891. A new locality for meteoritic iron with a preliminary notice of the discovery of diamonds in the iron. *American Journal of Science* 44:413–417.

Gilmour I., Russell S. S., Arden J. W., Lee M. R., Franchi I. A., and Pillinger C. T. 1992. Terrestrial carbon and nitrogen isotopic ratios from Cretaceous-Tertiary boundary nanodiamonds. *Science* 258:1624–1626.

Harris J. W. and Gurney J. J. 1979. In *The properties of diamond,* edited by Field J. E. New York: Academic Press. pp. 556–591.

Heider N. and Kenkmann T. 2003. Numerical simulation of temperature effects at fissures due to shock loading. *Meteoritics & Planetary Science* 38:1451–1460.

Hertzsch J. M., Ivanov B. A., and Kenkmann T. 2005. Numerical simulation of shock propagation in heterogeneous solids. In *Impact tectonics,* edited by Koeberl C. and Henkel H. Berlin-Heidelberg: Springer. pp. 423–445.

Hough R. M., Gilmour I., Pillinger C. T., Arden J. W., Gilkes K. W. R., Yuan J., and Milledge H. J. 1995. Diamond and silicon carbide in impact melt rock from the Ries impact crater. *Nature* 378:41–44.

Kenkmann T. 2003. *Processes of shock metamorphism and impact crater collapse.* Berlin: Habilitationsschrift Free University Berlin. 168 p.

Kenkmann T., Hornemann U., and Stöffler D. 2000. Experimental generation of shock-induced pseudotachylites along lithological interfaces. *Meteoritics & Planetary Science* 35:1275–1290.

Kenkmann T., Hornemann U., and Stöffler D. 2002. Transformation of graphite to diamond in shock experiments: A Raman study (abstract #1052). 33rd Lunar and Planetary Science Conference. CD-ROM.

Koeberl C., Masaitis V. L., Shafranovsky G. I., Gilmour I., Langenhorst F., and Schrauder M. 1997. Diamonds from the Popigai impact structure, Russia. *Geology* 25:967–970.

Lambert P. 1984. Shocked micas (abstract). 14th Lunar and Planetary Science Conference. pp. 413–414.

Langenhorst F. and Poirier J. P. 2000. Anatomy of black veins in Zagami: Clues to the formation of high-pressure phases. *Earth and Planetary Science Letters* 184:37–55.

Lewis R. S., Ming T., Wacker J. F., Anders E., and Steel E. 1987. Interstellar diamonds in meteorites. *Nature* 326:160–162.

Masaitis V. L. 1998. Popigai crater: Origin and distribution of diamond-bearing impactites. *Meteoritics & Planetary Science* 33:349–359.

Masaitis V. L., Shafranovsky G. I., and Federova I. G. 1995. The apographitic impact diamonds from astroblemes Ries and Popigai. *Proceedings of the Russian Mineralogical Society* 4:12–18.

Miyamoto M. 1998. Micro-Raman spectroscopy of diamonds in the Canyon Diablo iron meteorite: Implication for the shock origin. *Antarctic Meteorite Research* 11:171–177.

Müller W. F. and Hornemann U. 1969. Shock-induced planar deformation structures in experimentally shock-loaded olivines and in olivines from chondritic meteorites. *Earth and Planetary Science Letters* 7:251–264.

Schmitt R. T., Lapke C., Lingemann C. M., Siebenschock M., and Stöffler D. 2005. Distribution and origin of impact diamonds in the Ries Crater, Germany. In *Large meteorite impacts III*, edited by Kenkmann T., Hörz F., and Deutsch A. Boulder, Colorado: Geological Society of America. pp. 299–314.

Sobolev N. V. and Shatsky V. S. 1990. Diamond inclusions in garnets from metamorphic rocks: A new environment for diamond formation. *Nature* 343:742–745.

Stöffler D. 1971. Progressive metamorphism and classification of shocked and brecciated crystalline rocks at impact craters. *Journal of Geophysical Research* 76:5541–5551.

Stöffler D. 1982. Density of minerals and rocks under shock compression. In *Landolt-Börnstein. Numerical data and functional relationships in Science and Technology, New Series,* group 5, vol. 1. edited by Hellwege K. H. Berlin: Springer. pp. 120–183.

Stöffler D. and Langenhorst F. 1994. Shock metamorphism of quartz in nature and experiment: Basic observation and theory. *Meteoritics* 29:155–181.

Trunin R. F., Gudarenko L. F., Zhernokletov M. V., and Simakov G. V. 2001. *Experimental data on shock compression and adiabatic expansion of condensed matter.* Sarov, Russia: Russian Federal Nuclear Center-VNIIEF. 446 p.

Zhao X. Z., Cherian K. A., Roy R., and White W. B. 1998. Downshifts of Raman peak in diamond powder. *Journal of Material Research* 13:1974–1976.